Gold target fragmentation by 800 GeV protons

Article *in* Nuclear Physics A · July 1992

DOI: 10.1016/0375-9474(92)90555-X

Lembit Sihver
TU Wien

Kjell Aleklett
Uppsala University

Walter Loveland
Oregon State University

Henry Giacaman
Birzeit University

Nuclear Physics A543 (1992) 703–721
North-Holland

NUCLEAR
PHYSICS A

Gold target fragmentation by 800 GeV protons

L. Sihver[1] and K. Aleklett
University of Uppsala, Studsvik Neutron Research Laboratory, S-611 82 Nyköping, Sweden

W. Loveland
Dept. of Chemistry, Oregon State University, Corvallis, OR97331, USA

P.L. McGaughey
Los Alamos National Laboratory, Los Alamos, NM87545, USA

D.H.E. Gross and H.R. Jaqaman[2]
Hahn-Meitner-Institut Berlin, D-1000 Berlin 39, Germany

Received 8 July 1991
(Revised 26 February 1992)

Abstract: Target fragmentation formation cross sections, angular distributions, and range spectra were measured for the interaction of 800 GeV protons with ^{197}Au. From the measured formation cross sections, isobaric yields were deduced. The range distributions were converted to energy spectra. The angular distributions are sideward peaked for the fission/deep spallation products with the maxima in the distributions occurring at 30°–60°. The angular distributions and energy spectra are consistent with previous measurements of the interactions of energetic protons with gold. Within experimental uncertainties, the mass-yield distribution from the interaction of 800 GeV protons with gold is the same as from the interaction of 11.5 GeV protons with gold. The microcanonical model for statistical decay of very highly excited nuclei reproduces the general trend of the measured isobaric yields from the interaction of 800 GeV protons with ^{197}Au although the calculation predicts more structure in the yields than is observed.

E NUCLEAR REACTIONS: ^{197}Au(p, X); $E = 800$ GeV; measured σ for formation of 118 nuclides from ^{24}Na to ^{198}Au; measured fragment differential ranges and angular distributions; deduced $d\sigma/d\Omega\, dE$ (fragment Z, A) and isobaric yields.

1. Introduction

Studies of target fragmentation induced by very energetic projectiles [1-6]) have shown many unusual and interesting phenomena as the projectile energy increases. For example, the lab-frame angular distributions of the deep spallation products

Correspondence to: Professor W. Loveland, Radiation Center B123, Oregon State University, Corvallis OR97331-5903, USA.

[1] Present address: National Institute of Radiological Sciences, 4-9-1 Anagawa, Chiba-shi 260, Japan.
[2] Alexander von Humbolt Fellow; Permanent address: Birzeit University, Birzeit, West Bank.

($\Delta A(\equiv A_{target} - A_{product}) \geq 30$) and the intermediate mass fragments ($A_{fragment} < \frac{1}{3}A_{target}$) change from forward peaked to sideward peaked in p-heavy element interactions as the proton energy increases from approximately 3 to 10 GeV [refs. [2-6]]. Furthermore, Porile *et al.* have studied the interaction of 400 GeV protons with targets ranging from silver to gold. They found a similar change in the fragment angular distributions (from forward to sideward peaking) with increasing target mass number [7]. [Sideward-peaked angular distributions have also been observed for intermediate mass fragments (IMF) resulting from the interaction of 800 GeV protons with lanthanum, terbium, and lutetium [9]) and for IMF from the interaction [10]) of 25 GeV ^{12}C with ^{197}Au.] Forward (F) to backward (B) ratios of $F/B < 1$ for IMF were observed [1]) in the interaction of 13.6 GeV/nucleon ^{16}O with ^{197}Au.

Since little was known about the interaction of 800 GeV protons with heavy targets such as ^{197}Au, we measured the properties of the target fragments from this reaction. We report herein the measured values of the target fragment production cross sections, angular distributions and range distributions. From the target fragment production cross sections we deduced fragment mass distributions, and from the range distribution we deduced energy spectra. Our results are consistent with previous measurements of the interaction of lower energy protons with gold. We compare our measured fragment mass distributions with the predictions of the microcanonical model [11-13]) for the statistical decay of very highly excited nuclei.

2. Experimental techniques

The irradiations of the ^{197}Au targets were performed with 800 GeV protons at Fermilab. Inclusive measurements of the angular distributions and differential range spectra were made using radiochemical techniques that have been described previously [14-18]). To determine the target fragment yields, one irradiation, of approximately 9 h duration, was performed (total fluence 4.6×10^{13} protons). The ^{197}Au target thickness for this irradiation was 50.1 mg/cm^2. No catcher foils were used in this irradiation. Another irradiation, of approximately 70 h duration, was performed to determine angular distributions and differential range spectra. Target thicknesses were 0.24 and 0.22 mg/cm^2, respectively. The beam intensity was determined for each irradiation by two secondary electron monitors [19]), which agreed within errors. Their calibrations were based upon a measured Cu(p, X) ^{24}Na cross section of 3.9 mb at 400 GeV [ref. [19])] which was assumed to be constant between 400 and 800 GeV. [A recent measurement [45]) has confirmed this energy independence between 30 and 800 GeV, but with a cross section value that is 8% lower than that reported in ref. [19])]. The experimental setup for determining the angular distributions consisted of the gold target mounted at 45° to the beam direction. Fragments emerging from the target were caught in 125 μm Mylar foils ($5° < \theta < 35°$) or 100 μm Mylar foils ($35° < \theta < 171°$). Following irradiation, the catcher foils were divided into nine pieces corresponding to the angular intervals of (a) 5°–13°; (b) 13°–23°; (c) 23°–35°;

(d) 35°–52°; (e) 52°–76°; (f) 76°–104°; (g) 104°–128°; (h) 129°–158° and (i) 158°–171°. The effect of "target shadowing" was such that the "useful" solid angles corresponding to these angular ranges were 0.125, 0.345, 0.614, 0.931, 1.18, 1.16, 1.18, 1.45 and 0.271 sr, respectively. Foils (b), (d), (f) and (h) were counted on a high-efficiency Ge detector while foils (a), (c), (e), (g) and (i) were counted on a lower efficiency detector. As a consequence, values of $d\sigma/d\Omega\ (\theta)$ are reported for angular intervals (b), (d), (f) and (h) for all radionuclides while values of $d\sigma/d\Omega(\theta)$ for the other angular intervals could only be measured occasionally.

The stack of Mylar foils for determining the differential range spectra was also mounted in a cylindrical geometry. To determine the fragment differential range spectra, two stacks of Mylar foils were mounted inside the cylindrical scattering chamber (diameter ~30 mm) at 90° with respect to the incident beam. The catcher foils subtended angles of 72°–108° in the reaction plane and an azimuthal angle of 45° in the plane normal to the beam direction. Thus the geometry of the catcher foils was such that ~25% of the recoils in the angular interval were collected. Since the foil stacks were mounted on the walls of the cylindrical scattering chamber, the fragments emerging from the target entered the foils normal to the surface. The target was tilted at 45° to ensure no portion of the foil stack was "shadowed". The assay of the radioactivity in the Mylar foils and the target foils from the two experiments was begun within less than two days after the end of the irradiations. The foils were counted without chemical separation using off-line γ-ray spectroscopy to follow the decay of the individual nuclide γ-rays. The resulting γ-ray spectra were analyzed using the interactive analysis program DECHAOS [20]). The analysis of the decay curves and the assignment of the radionuclides present and their activities were done in similar manner to that described previously [17]). The radioactive decay data used in these assignments was an updated form [21]) of the Reus-Westmeier tables [22]).

3. Experimental results

3.1. TARGET FRAGMENT YIELDS

The target fragment formation cross sections were calculated from end of bombardment radionuclide activities [17]). Thus, in calculating the formation cross sections, a correction is made for any radioactive decay that occurred after the end of irradiation but no correction is made for any feeding during the irradiation. No catcher foils were used in the thick target experiment for determining the target fragment production cross sections. The measured target fragment production cross sections were corrected for the fractions of activity recoiling out of the target. The percentage recoil loss was assumed to be the same as for the interaction of 300 GeV protons with gold [23]). Thus for ^{24}Na, $\sigma_{\rm meas} = 9.68$ mb; $(F+B)$ from ref. [23]) is 0.25; and $\sigma_{\rm corr} = 12.9$ mb. The recoil loss decreases smoothly with fragment mass number.

For $A_{frag} < 28$ the correction was ~25%, for $43 \leq A_{frag} \leq 56$ it was ~14%. For $58 \leq A_{frag} \leq 86$ the recoil correction ranged from 13% ($A = 58$) to 8% ($A = 86$) with an average value of 10%. For $88 \leq A_{frag} \leq 105$ the recoil correction ranged from 8% ($A = 88$) to 6% ($A = 105$) with an average value of 7%. For nuclides with $A > 110$ the recoil loss was assumed to be negligible.

The measured target fragment production cross sections, after correction, are tabulated in table 1. The errors reflect the uncertainties due to counting statistics. In fig. 1 we show how our values of the production cross sections compare with previous measurements from energetic proton-gold collisions [24,25,27]). Our data confirm that limiting fragmentation behavior (i.e. the cross sections become roughly independent of beam energy above some minimum energy) occurs, with an onset at ~10 GeV. The limiting fragmentation behavior has previously also been observed for heavy-ion reactions [26]), for which the onset is at ~2.1 GeV/nucleon. Kaufman *et al.* [27]) showed that the ratios of the cross sections measured for the interactions of 300 and 11.5 GeV protons with gold vary regularly with mass number. They found that the ratio $\sigma(300)/\sigma(11.5)$ decreases from about 1.1 for the lightest fragments to about 0.9 for nuclides in the range $121 \leq A_{frag} \leq 185$. Our measured cross sections at 800 GeV agree with that trend. This relative independence of the fragment production cross sections from the projectile energy implies the spectrum of excitation energies of the initial target-like fragment is not dependent on projectile energy.

The mass-yield distribution was deduced from the cross sections tabulated in table 1, using an estimation procedure discussed previously [16]). The nuclidic formation cross sections were placed in nine groups according to mass number. These cross sections were corrected for precursor beta decay, where necessary, by assuming the independent yield cross sections for a given species, $\sigma(Z, A)$, can be expressed as a function of the isobaric yield $\sigma(A)$ as:

$$\sigma(Z, A) = \sigma(A)[2\pi C_z^2(A)]^{-1/2} \exp[-(Z - Z_{m.p.})^2/2C_z^2(A)], \qquad (1)$$

where $C_z(A)$ is the gaussian width parameter for mass number A and $Z_{m.p.}(A)$ is the most probable atomic number for that A. Using this assumption and the further assumption that $\sigma(A)$ varies slowly and smoothly as a function of A (allowing data from adjacent isobars to be combined in determining $Z_{m.p.}(A)$ and $C_z(A)$), one can use the laws of radioactive decay to correct iteratively the measured cumulative formation cross sections for precursor decay.

Within each of the nine groups, the data were fitted to a gaussian-shaped independent yield distribution. The centers of the charge distributions were represented by a polynomial function of the second order in A over a limited range in A. Variation of $Z_{m.p.}$ with mass number is generally smooth except for the region with $A > 190$ where $\sigma(A)$ is not varying slowly with A and the deduced independent yield data do not generally constrain $Z_{m.p.}$ very well. Nuclides with isomer or other feeding problems were not included in the analysis. The nuclidic groupings along with the centers and widths of the gaussian distributions are given in table 2. The independent

TABLE 1

Formation cross sections (mb) of nuclides formed in the reaction of 800 GeV protons with ^{197}Au

Nuclide	Cross section	Nuclide	Cross section	Nuclide	Cross section
^{24}Na	12.9 ± 1.4	^{99}Mo	0.38 ± 0.03	^{165}Tm	11.9 ± 2.0
^{28}Mg	3.4 ± 0.5	^{100}Pd	1.54 ± 0.07	^{166}Yb	9.3 ± 1.3
^{43}K	2.5 ± 0.4	^{100}Rh	2.4 ± 0.2	^{167}Tm	13.6 ± 0.1
^{44}Sc^{m}	2.1 ± 0.3	^{101}Rh^{m}	5.7 ± 0.1	^{169}Yb	10.1 ± 0.3
^{46}Sc	5.7 ± 0.3	^{105}Ag	5.5 ± 0.1	^{169}Lu	10.5 ± 2.4
^{47}Sc	4.0 ± 0.3	^{105}Rh	1.7 ± 0.2	^{170}Hf	7.4 ± 0.6
^{47}Ca	0.55 ± 0.02	^{106}Ag^{m}	1.4 ± 0.1	^{170}Lu	13.5 ± 0.9
^{48}Sc	1.4 ± 0.1	^{111}In	4.6 ± 0.3	^{171}Hf	8.5 ± 0.4
^{48}V	1.7 ± 0.1	^{113}Sn	5.7 ± 0.2	^{171}Lu	15.6 ± 0.5
^{51}Cr	4.5 ± 0.2	^{119}Te	5.4 ± 0.2	^{172}Er	2.4 ± 0.2
^{52}Mn	0.91 ± 0.11	^{120}Sb^{b}	0.11 ± 0.01	^{173}Hf	13.2 ± 0.9
^{54}Mn	5.9 ± 0.2	^{121}Te	7.0 ± 0.1	^{175}Hf	13.3 ± 0.2
^{56}Co	0.58 ± 0.08	^{121}Te^{m}	0.26 ± 0.03	^{175}Ta	11.2 ± 0.6
^{57}Co	2.3 ± 0.1	^{122}Xe	5.2 ± 0.4	^{176}Ta	18.4 ± 0.5
^{58}Co	4.6 ± 0.1	^{123}I	3.7 ± 0.6	^{177}Ta	14.4 ± 0.2
^{59}Fe	1.9 ± 0.1	^{123}Te^{m}	1.1 ± 0.3	^{177}Lu^{m}	1.5 ± 0.1
^{67}Ga	3.2 ± 0.1	^{125}Xe	6.3 ± 0.4	^{178}W	11.9 ± 0.1
^{69}Zn^{m}	0.95 ± 0.10	^{126}Sb	0.11 ± 0.04	^{181}Hf	0.95 ± 0.09
^{71}As	2.3 ± 0.1	^{127}Xe	5.6 ± 0.3	^{181}Re	12.0 ± 0.2
^{72}Ga	2.7 ± 0.1	^{128}Ba	7.1 ± 0.4	^{182}Os	12.8 ± 0.5
^{74}As	2.5 ± 0.1	^{129}Cs	8.0 ± 1.0	^{183}Re	18.9 ± 0.6
^{75}Se	4.1 ± 0.3	^{131}Ba	7.7 ± 0.7	^{183}Os^{m}	5.7 ± 0.2
^{77}Br	3.8 ± 0.8	^{135}Ce	7.4 ± 1.6	^{183}Os	8.8 ± 0.2
^{82}Sr	1.7 ± 0.2	^{143}Pm	10.6 ± 0.3	^{185}Ir	7.1 ± 0.6
^{83}Rb	7.3 ± 0.4	^{145}Eu	8.5 ± 0.5	^{185}Os	21.4 ± 0.3
^{83}Sr	3.3 ± 0.1	^{146}Gd	8.5 ± 1.0	^{186}Ir	6.1 ± 0.1
^{84}Rb	2.3 ± 0.1	^{147}Eu	10.7 ± 1.8	^{187}Ir	18.3 ± 2.5
^{85}Sr	7.1 ± 0.1	^{147}Gd	7.4 ± 0.4	^{188}Ir	3.8 ± 0.3
^{86}Y	2.6 ± 0.6	^{148}Pm^{m}	0.4 ± 0.1	^{188}Pt	15.7 ± 0.2
^{87}Y^{m}	7.8 ± 0.5	^{149}Gd	10.6 ± 0.6	^{189}Ir	21.1 ± 0.4
^{87}Y	7.1 ± 0.4	^{151}Tb	4.4 ± 0.6	^{189}Pt	25.0 ± 1.4
^{88}Zr	4.7 ± 0.1	^{151}Gd	7.3 ± 0.7	^{190}Ir	2.8 ± 0.7
^{88}Y	2.4 ± 0.1	^{152}Tb	6.2 ± 0.3	^{191}Pt	19.5 ± 0.9
^{89}Zr	6.6 ± 0.1	^{153}Tb	7.8 ± 0.4	^{192}Ir	2.3 ± 0.2
^{95}Tc	5.2 ± 0.1	^{153}Gd	7.7 ± 0.4	^{193}Au	10.6 ± 0.5
^{95}Nb	0.84 ± 0.01	^{155}Tb	10.3 ± 0.2	^{194}Au	19.2 ± 0.6
^{95}Nb^{m}	0.3 ± 0.1	^{155}Dy	6.0 ± 0.2	^{194}Ir	3.6 ± 0.9
^{96}Tc	2.1 ± 0.1	^{157}Dy	9.2 ± 0.2	^{196}Au	64.7 ± 4.7
^{97}Ru	3.9 ± 0.4	^{160}Er	9.9 ± 0.5	^{198}Au	40.9 ± 0.3

yield distributions estimated from the measured formation cross sections are shown in fig. 2.

In fig. 3, we compare the deduced $Z_{\mathrm{m.p.}}(A)$ and $C_z(A)$ functions with those deduced previously [27]) for the interaction of 11.5 GeV protons with gold and the systematics of proton–nucleus collisions deduced by Rudstam [28]). Our data appears to be consistent with the systematics of Rudstam [28]) although there are differences

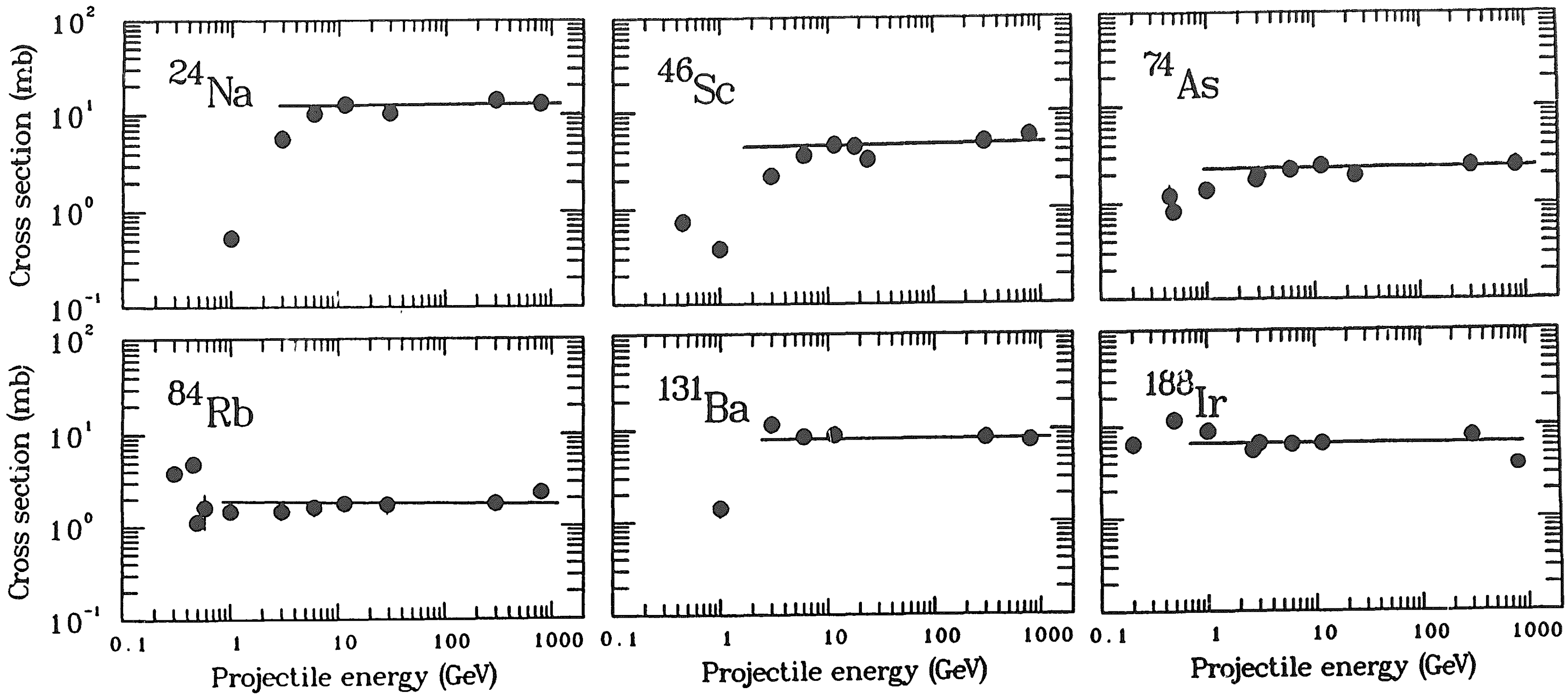

Fig. 1. Excitation functions for target fragments produced in energetic proton-gold collisions [24,25,27]). The solid lines serve to guide the eye through the data.

TABLE 2

Charge dispersion parameters

Fragment mass number range	$Z_{m.p.}(A)$	$C_z(A)$
24–59	$0.466A-0.38$	0.5
65–77	$-0.382\times10^{-3}A^2+0.483A+0.000$	0.6
82–89	$-0.382\times10^{-3}A^2+0.483A-0.000$	0.6
95–113	$-0.382\times10^{-3}A^2+0.483A-0.200$	0.9
122–129	$-0.382\times10^{-3}A^2+0.483A+0.231$	0.6
131–160	$-0.382\times10^{-3}A^2+0.483A+0.562$	0.6
165–178	$-0.382\times10^{-3}A^2+0.483A+0.254$	0.6
181–189	$-0.382\times10^{-3}A^2+0.483A+0.306$	0.5
191–198	$-0.382\times10^{-3}A^2+0.483A-1.15$	0.6

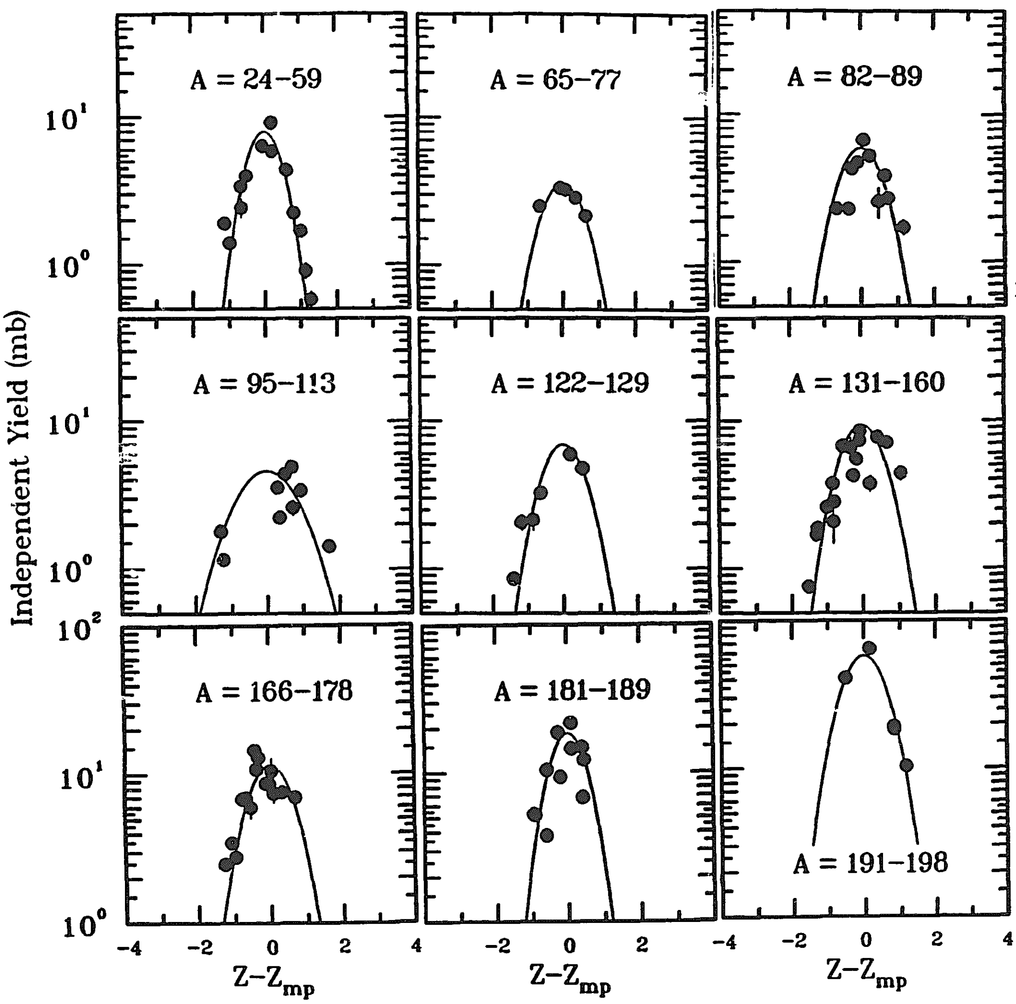

Fig. 2. The independent yields distributions from the interaction of 800 GeV protons with ^{197}Au. The plotted points are the independent yield cross sections calculated from the data while the solid line are the gaussian charge dispersions used in the calculation.

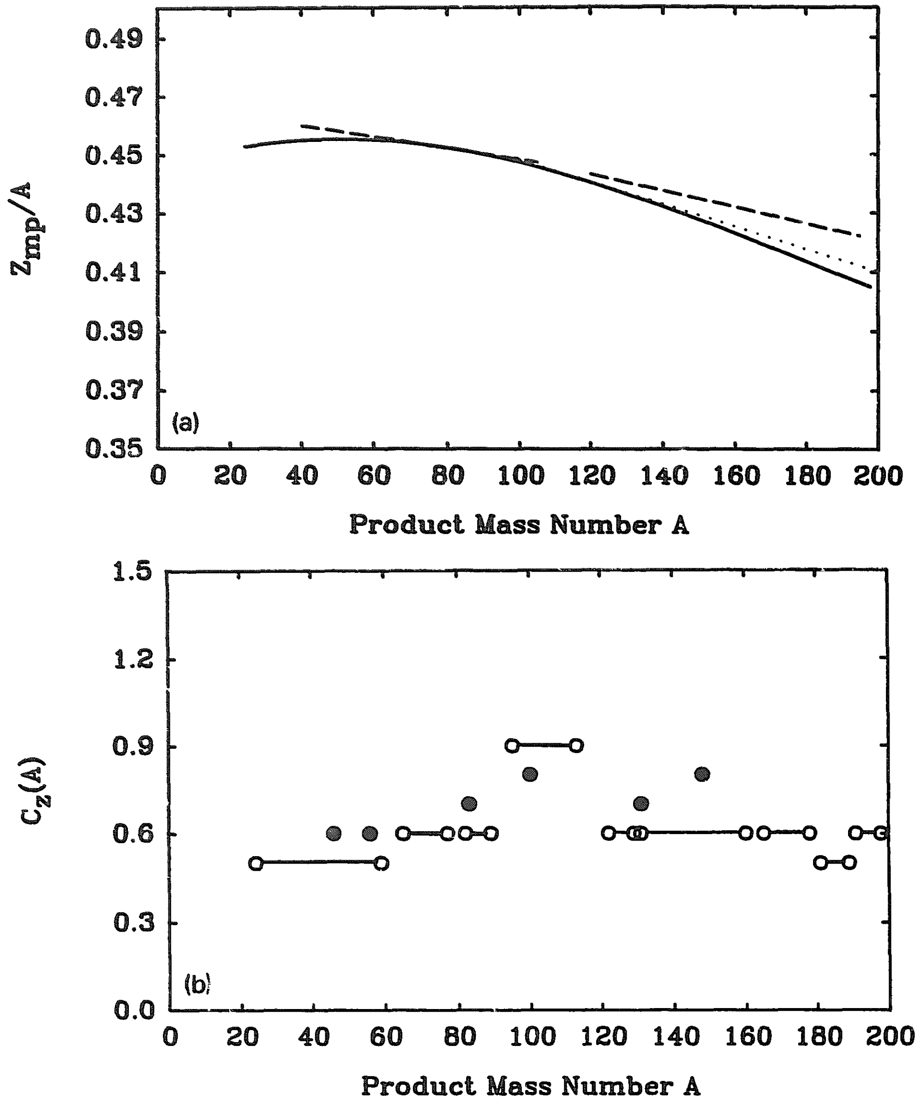

Fig. 3. (a) Variation of $Z_{m.p}/A$ versus A. Solid line, this work; dashed line, ref. [27]); dotted line, ref. [28]). (b) Variation of $C_z(A)$ versus A. Open circles, this work; closed circles, ref. [27]).

between our $Z_{m.p.}$ data and the $Z_{m.p.}$ values deduced by Kaufman *et al.* [27]), especially at large A-values. It is difficult to assess the uncertainties in the values of $Z_{m.p.}(A)$ and $C_z(A)$ deduced in this type of analysis and thus to attach any significance to the discrepancies noted.

The target fragment isobaric yields are shown in fig. 4, together with the fragment isobaric yield distribution from the reaction of 11.5 GeV protons with ^{197}Au deduced by Kaufman *et al.* [25,27]). Within experimental uncertainties, the mass-yield from the reaction of 800 GeV protons with gold is the same as from the reaction of 11.5 GeV protons with gold [25,27]) in accord with limiting fragmentation. For the isobaric yield distribution for the reaction of 800 GeV protons with ^{197}Au, the error bars on the integrated data points primarily reflect the uncertainties due to the fitting process [16]) (~30%). The deduced isobaric yield data for $A \geq 191$ is more uncertain due to the

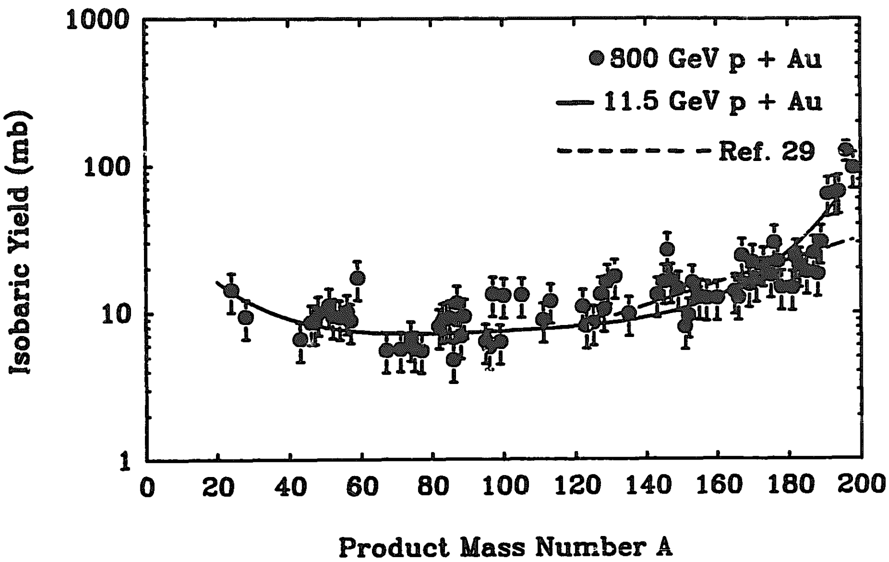

Fig. 4. Isobaric yield distribution for the fragmentation of the fragmentation of ^{197}Au by 800 GeV p, and 11.5 GeV p [ref. [27])]. The calculated isobaric yield for the spallation products, using the expression derived by Rudstam [28]), and an exponential slope constant according to Sümmerer and Morrissey [29]) is also shown.

breakdown of the assumption of $\sigma(A)$ varying slowly with A and the relatively small number of measurements.

In fig. 4 we also show calculated the isobaric yield $Y(A)$ for spallation products, using the expression originally derived by Rudstam [28]) and recently used by Sümmerer and Morrissey [29])

$$Y(A)=\sigma_R P \exp[-P(A_t-A)], \tag{2}$$

where σ_R is the total reaction cross section [1790 mb, ref. [30])]. The slope constant P was parameterized [29]) by an exponential which depends only on the target mass A_t:

$$\ln P=-7.57\times 10^{-3}A_t-2.584 \tag{3}$$

The calculated mass yield for the spallation products from the interaction of 800 GeV protons with gold is in good agreement with the experimental yields. Thus, the product mass distribution for the 800 GeV p+Au reaction is consistent with what we know about product mass distributions in p-nucleus collisions.

3.2. TARGET FRAGMENT ENERGY SPECTRA

The measured differential range spectra were converted to energy spectra using standard range-energy tables [31]). Corrections for energy loss in the gold target were made by assuming that, on the average, the fragments traversed $\frac{1}{2}(0.22\ \mathrm{mg/cm^2})/\cos 45°$ in the target. This thickness was converted to the Mylar equivalent on the basis of the relative stopping powers of Mylar and gold [31]).

In fig. 5, we show representative target fragment energy spectra from the stack mounted at ~90°. In the same figure, we also show the shape of the energy spectrum for the fragment mass bins $28 \leq A \leq 31$, $80 \leq A \leq 89$ and $120 \leq A \leq 139$ from the interaction of 4.9 GeV protons with gold [32,33]. All products (except the intermediate mass fragments such as ^{47}Sc) from the interaction of 800 GeV protons with gold show the expected pseudo-exponential spectra characteristic for deep spallation products. The slope of the spectra becomes greater as the fragment mass increases.

The two-step vector model of high-energy reactions assumes that in the first step of the reaction the incident proton interacts with the target nucleus. The proton imparts a velocity $v_{\parallel}$ along the beam direction to the resulting residual nucleus. The

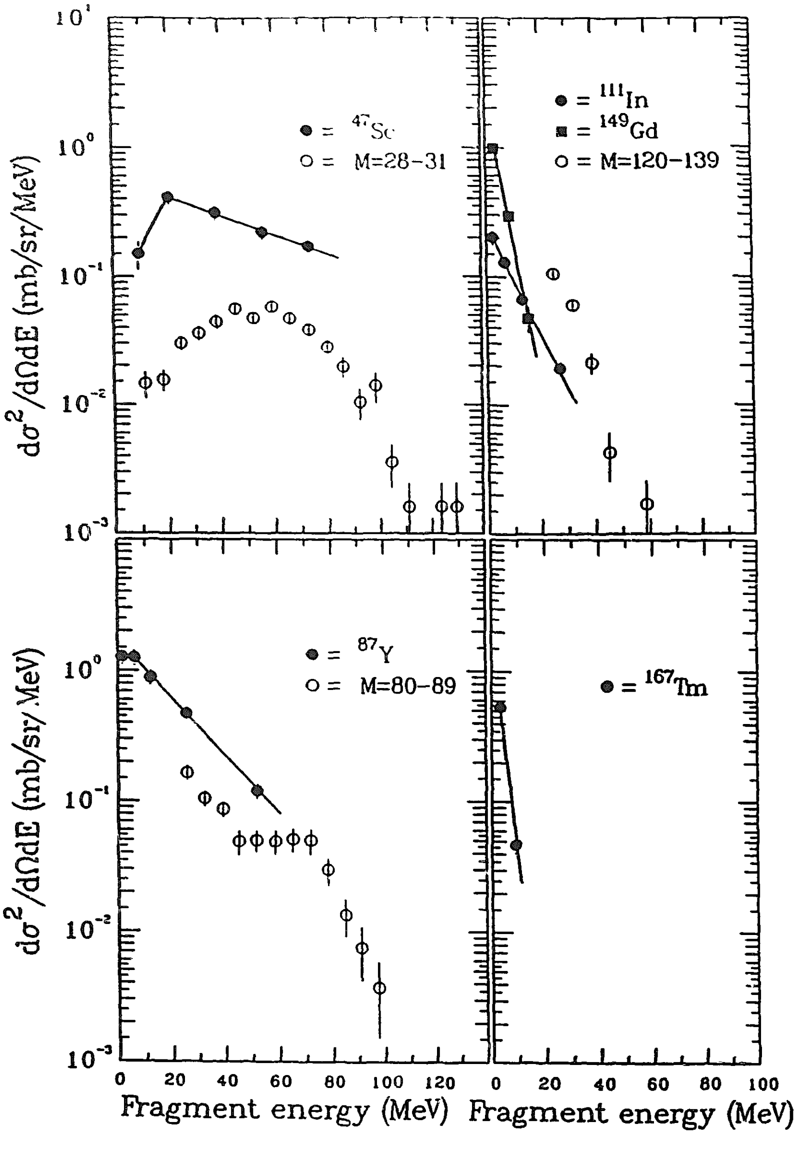

Fig. 5. Target fragment energy spectra from the Mylar stack mounted at ~90°, and the shape of the energy spectra for the fragment mass bins $28 \leq A \leq 31$, $80 \leq A \leq 89$ and $120 \leq A \leq 139$ from the interaction of 4.9 GeV protons with gold [32].

breakup of this remnant leads to isotropic emission in the moving system of a fragment with velocity V. The kinetic energy of the fragment in the moving system is $T=\frac{1}{2}AV^2$. The forward motion from the first step of the reaction has a small effect on measurements at 90°, which can be disregarded. This means that our calculated mean fragment energies at 90° can be treated as the mean recoil kinetic energies, $\langle T\rangle$, in the moving system, if the two-step vector model is valid. The average recoil momenta are then calculated as:

$$P_{\mathrm{r.m.s.}}=(2A_{\mathrm{obs}}\langle T\rangle 931.5)^{1/2} \quad [\mathrm{MeV}/c]\,. \tag{4}$$

The mean energies and the average recoil momentum of some representative products are tabulated in table 3.

A velocity spectrum of ^{149}Gd from the interaction of 800 GeV protons with gold was calculated from the measured range distribution. This velocity spectrum is shown in fig. 6 together with the velocity spectrum of ^{149}Tb from the fragmentation of gold by 2.2 GeV protons, measured by Crespo *et al.* [34]). The two spectra have the same shape. We thought it would be interesting to see to what extent the shapes of the spallation product spectra could be predicted by conventional models for high energy processes. Accordingly, we assumed we had a group of ^{197}Au nuclei with an excitation energy distribution given by fig. 10. Neglecting any momentum imparted to these nuclei in the primary nucleon-target interaction (which is appropriate for the nuclei detected at 90°), we calculated the energy spectra of the spallation residue nuclei due to particle evaporation (considering possible de-excitation by fission). The calculations were performed using a modified DFF procedure [35]). A representative calculated fragment spectrum (for $A=145$–155) is compared to the data in fig. 6. There appears to be excellent agreement between the measured and calculated spectra, suggesting these spallation product spectra can be simply accounted for using conventional models of high energy processes.

The isotropic component of the target residue momentum is often thought to be produced by a random combination of small recoil momenta from sequential evaporation, i.e. a random walk in recoil momentum space [35]). Crespo *et al.* [34]) have

TABLE 3

Mean fragment energies and average recoil momenta for some representative products

Nuclide	$\langle T\rangle$ [MeV]	$P_{\mathrm{r.m.s.}}$ [MeV/c]
^{47}Sc	50.7	2110
^{87}Y	18.6	1740
^{97}Ru	10.2	1360
^{111}In	10.4	1470
^{149}Gd	5.2	1200
^{153}Tb	4.6	1140
^{167}Tm	3.9	1100

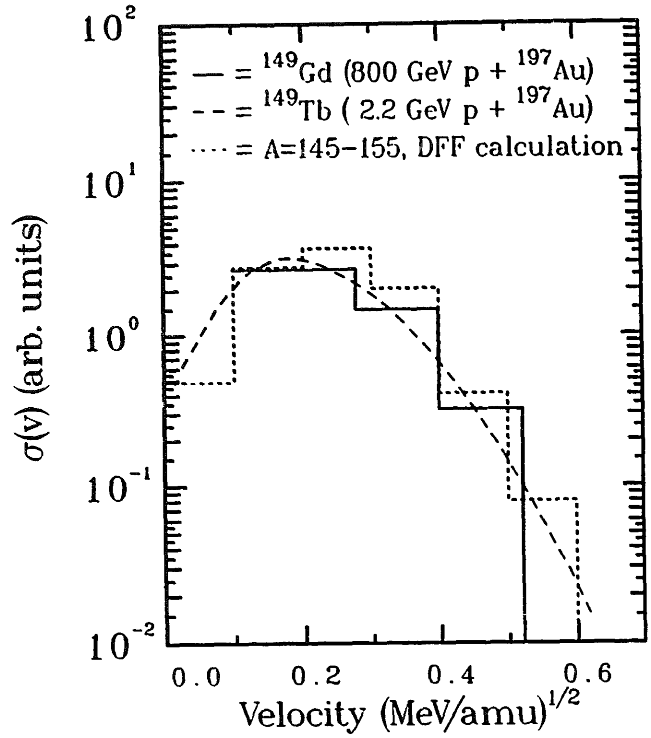

Fig. 6. Velocity spectrum of ^{149}Gd from the interaction of (a) 800 GeV p, (b) 2.2 GeV p with ^{197}Au [ref. [34])]. Also shown is a DFF calculation of the velocity spectra of similar products from the 800 GeV p+Au reaction.

shown that a sequential evaporation chain in which the residue receives an average momentum in each step, $\langle P_i \rangle$, which leads to the expression:

$$P_{\mathrm{r.m.s.}} \equiv A_{\mathrm{frag}} \langle V^2 \rangle^{1/2} \approx \langle P_i \rangle (\Delta A)^{1/2} = (A_{\mathrm{frag}} \langle p_i \rangle (\Delta A)^{1/2}) / A_{\mathrm{avg}} , \tag{5}$$

where A_{avg} is the average mass number of the residue in the chain, $\Delta A = A_t - A_{\mathrm{frag}}$, and $\langle p_i \rangle$ is the average momentum of the emitted particles.

It has been shown [23,36-40]) that the momentum distributions of projectile and target residues from many reactions of relativistic projectiles with a broad range of targets are quantitatively consistent. The values of $P_{\mathrm{r.m.s.}}$ depend linearly on the square root of the mass loss. In fig. 7 the values of $P_{\mathrm{r.m.s.}}$ for the fission/deep spallation products from the interactions of 800 GeV protons with gold are shown as a function of the observed mass loss $\Delta A = A_t - A_{\mathrm{frag}}$, together with data from Morrissey [36]). A line is drawn through the data in fig. 7 with a slope of 150 MeV/c/u$^{1/2}$ representing the semiempirical dependence $P_{\mathrm{r.m.s.}} = 5.1(\Delta A)^{1/2}$ [MeV/u]$^{1/2}$, discussed in ref. [36]). The data from the interaction of 800 GeV protons with gold is in good agreement with the systematics.

3.3. TARGET FRAGMENT ANGULAR DISTRIBUTIONS

In fig. 8, we show some representative target fragment lab-frame angular distributions. The differential cross sections are normalized to unity at 90°. The ^{47}Sc angular

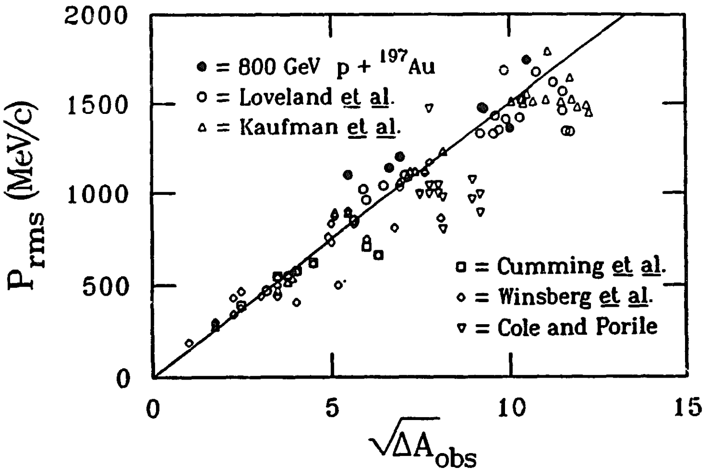

Fig. 7. The recoil momentum, $P_{\mathrm{r.m.s.}}$, as a function of observed mass loss from target residues [36]). The straight line with a slope of 150 MeV/c/$u^{1/2}$ represents a previous semiempirical description discussed in ref. [36]).

distribution is sideward peaked. For the fission/deep spallation products (A = 87–111), the distributions are also sideward peaked with the maxima in the distributions occurring at angles between 30°–60°. The heavier spallation products have forward-peaked distributions. Wang and Porile [9]) have pointed out that the fragment angular distributions from reactions induced by energetic protons can be parameterized as:

$$F_L(\Theta_L) = 1 + A_1 \cos \Theta_L + A_2 \cos^2 \Theta_L . \tag{6}$$

The solid curves in fig. 8 represent least-squares fits to the data using eq. (6). The values of the coefficients A_1 and A_2 are tabulated in table 4. From eq. (6) we get that A_1 is a measure of the forward-backward asymmetry; $A_1 = 2(F - B)$, where F and B are the forward and backward fractions of the differential cross section, respectively. The parameter A_2 is a measure of the anisotropy of the angular distribution. A positive A_2 value indicates that the differential cross section at 90° is smaller than the average of the values at 0° and 180°, while a negative A_2 value indicates the opposite. The A_1 and A_2 derived from fitting the present data agree with the systematics [9]) (shown in fig. 9a and 9b) of the variations of A_1 and A_2 with mass difference between target and product. The asymmetry and the anisotropy parameters decrease with increasing ΔA. A_2 becomes negative for sufficiently large mass losses, where the laboratory angular distributions are sideward peaked.

4. Comparison of data to theory

4.1. MASS DISTRIBUTIONS

In a series of recent papers Gross *et al.* [11-13]) have shown that a realistic microcanonical simulation of all important decay channels of highly excited nuclei is

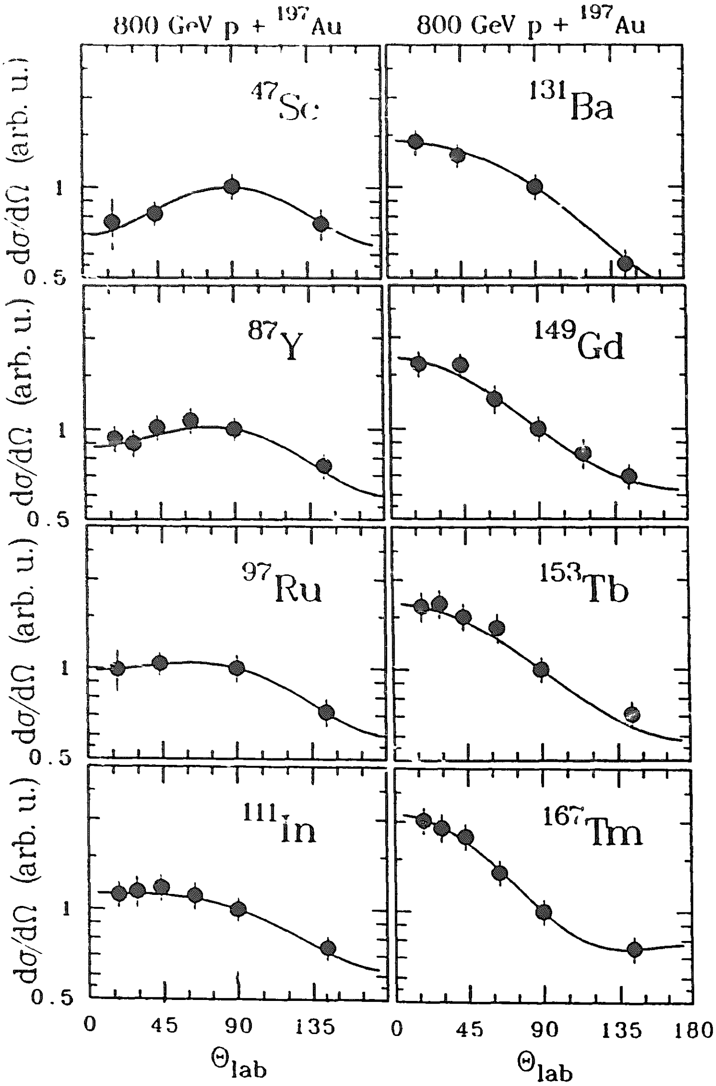

Fig. 8. Target fragment laboratory angular distributions from the interaction of 800 GeV protons with ^{197}Au. The solid curves represent least squares fits to the data using eq. (6).

TABLE 4

Parameters derived from fits to the angular distributions from the interaction of 800 GeV protons with ^{197}Au

Product	A1	A2
^{47}Sc	0.024 ± 0.028	−0.331 ± 0.060
^{87}Y	0.135 ± 0.029	−0.262 ± 0.055
^{97}Ru	0.189 ± 0.006	−0.207 ± 0.013
^{111}In	0.250 ± 0.023	−0.122 ± 0.004
^{131}Ba	0.485 ± 0.034	−0.049 ± 0.070
^{149}Gd	0.541 ± 0.054	0.168 ± 0.110
^{153}Tb	0.540 ± 0.044	0.123 ± 0.084
^{167}Tm	0.668 ± 0.032	0.445 ± 0.061

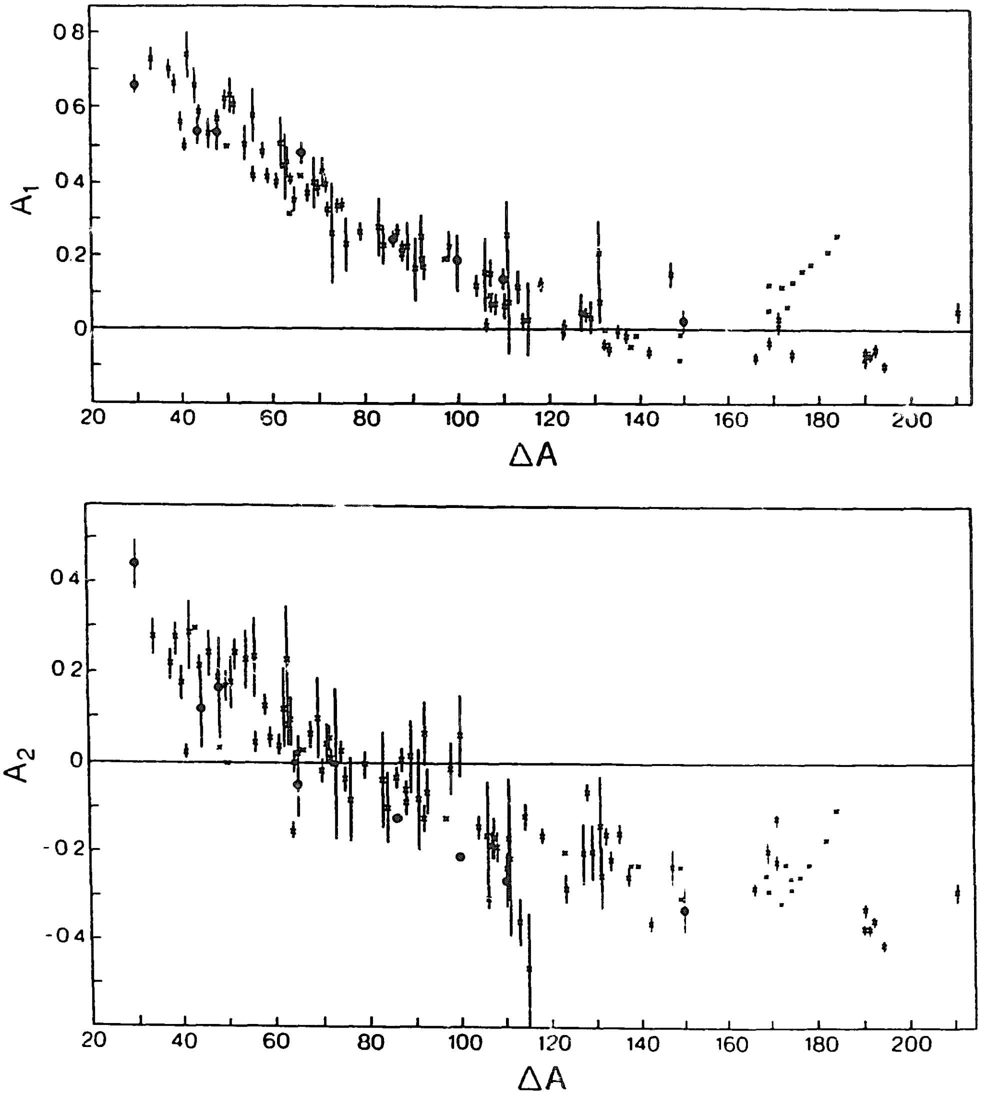

Fig. 9. (a) Variation of the asymmetry parameter A_1 with mass loss ΔA for deep spallation products and fragmentation products of the interaction of high-energy protons [$T_p \geq 30$ GeV, ref. [9]] with silver (star), lanthanum (cross), terbium (triangle), lutetium (square), gold (fancy cross), and uranium (diamond). The results for fragments from the interaction of 800 GeV protons with gold are shown as filled circles. Error bars are shown where available. This figure is taken from ref. [9]). (b) Variation of the anisotropy parameer A_2 with mass loss ΔA for deep spallation products and fragmentation products [9]). See part (a) for details.

possible. We thought it would be appropriate to compare our data for the 800 GeV proton + ^{197}Au reaction with the predictions of this model.

With the mass yield $\sigma(E^*, A)$ given by the microcanonical simulation, the total mass yield is

$$\sigma(A) = \int \sigma(E^*, A) P(E^*) \, dE^* . \tag{7}$$

The probability $P(E^*)$ that the target nucleus receives excitation energy E^* can be calculated within the Glauber multiple scattering theory [13]). This probability is

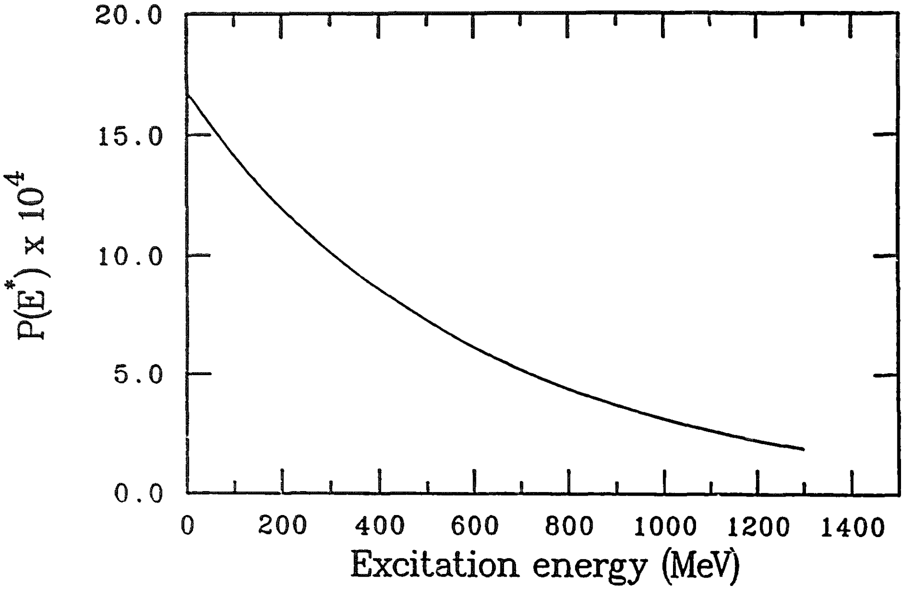

Fig. 10. The probability, $P(E^*)$, of excitation energy E^* of the target remnant, as given by Glauber multiple scattering theory. As suggested by ref. [41]), we took $P(E^*)$ = constant for $1.2 \leq E^* \leq 2.0$ GeV and set $P(E^*) = 0$ for $E^* > 2$ GeV.

shown in fig. 10. The result of our calculation, shown in fig. 11, is in rough overall agreement with our measured mass yield distribution. There is, however, considerable more structure in the calculated yields which is not observed. This failure to observe structure in fragment mass yield distributions predicted by the microcanonical simulation has been noted by others [42]).

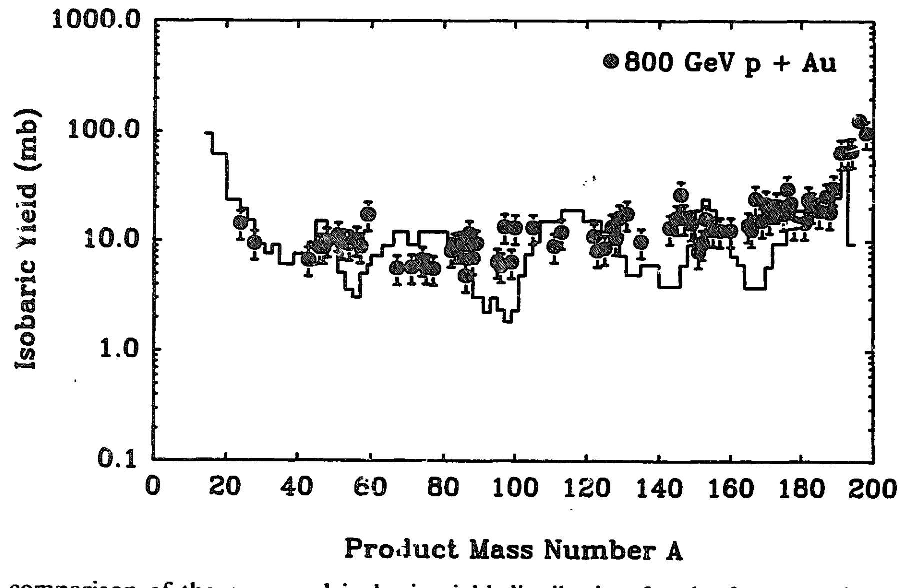

Fig. 11. A comparison of the measured isobaric yield distribution for the fragmentation of ^{197}Au by 800 GeV protons with that calculated (histogram) using the microcanonical model for statistical decay of very highly excited nuclei presented by Gross *et al.* [11-13]).

To review the uncertainties in the model which may be responsible for this structure, we note the fundamental assumption in the model is that most fragments are produced from an equilibrated source. This is not guaranteed in reality, although recent observations suggest multifragmentation events come from an equilibrated source. However, it is useful to remember the reasons for this assumption.

At excitation energies of the order of the binding energy, heavy nuclei cannot decay into free nucleons. The reason is simple. At birth the fragments are still in proximity and because of the long-range Coulomb interaction there is considerable Coulomb energy. This can only be available if most of the nucleons cluster together in different intermediate mass nuclei and gain binding energy. Therefore, at these excitation energies the production of intermediate mass nuclei is the predominant decay mode. To have a chance to describe these decays realistically, a theory has to incorporate cluster formation explicitly. Currently, there is no dynamical theory starting from a description of interacting nucleons which is able to do this [43]). Thus, in formulating the microcanonical model, Gross *et al.* assumed equilibrium and neglected any dynamics. However, this assumption is not unreasonable. Equilibrium decay takes care of the constraints of the reaction by the global conservation laws and by phase space. These are certainly the most important factors.

There are two free parameters in this calculation:

(i) The radius of the freeze-out geometry for ^{197}Au, $R_0 = 2.2A^{1/3}$ fm. This value was determined in a fit of the distribution of relative velocities of intermediate mass fragments after the collision of 800 MeV/nucleon alpha particles with gold [44]). As the relative velocity is a direct measure of the Coulomb acceleration and therefore of the charge distribution, we believe this value of R_0 to be fairly well determined. Of course, there might be a difference in the freeze out configuration reached after a collision of an 800 MeV/nucleon alpha particle with Au, compared to that of an 800 GeV proton.

(ii) The distribution $P(E^*)$ of excitation energies is very uncertain. The shape of the excitation energy spectrum at low excitation seems to be similar for the Glauber theoretical distribution and for the empirical form used here. However, we don't have a precise knowledge of the spectrum at high excitations; in particular, we don't know how far in E^* the excitation energy spectrum reaches. Varying the high-energy cut-off shifts the relative yield for fragments with $A > 100$ compared to the lighter fragments. This is a smooth effect as the mass yield $\sigma(A)$ is the product of the total proton-gold cross section σ_{total} times the probability $P(A)$ times the average multiplicity $\langle m \rangle$. At higher excitation energy $P(A > 100)/P(A < 100)$ drops but $\langle m \rangle$ rises. In the calculations here we assumed a distribution of excitation energies as given in fig. 10 between $E^* = 50$ MeV and $E^* = 2$ GeV. Of course, the distribution of excitation energies might be different in the limiting fragmentation region (bombarding energies above 10 GeV) compared to proton energies of 1-2 GeV in the Glauber theory.

A third weak point of the model is the treatment of the secondary (delayed) evaporation of charged particles (protons and α-particles), in a rough and schematic fashion only. The reason for this is that delayed charged-particle emission demands the simultaneous treatment of the Coulomb trajectories of all interacting charged fragments because of the long range of the Coulomb interaction. This, however, goes far beyond the computer capacity available to us. We have ignored delayed charged-particle evaporation and assumed that alpha-particle emission is rather fast and that nuclei leaving the freeze-out configuration decay only by neutron evaporation. Delayed alpha-particle emission by the heavier fragments might wash out the structures in the mass yield distribution calculated within the present model.

In view of the general reproduction of the overall shape of the mass yield and of the absolute value of the cross section, the microcanonical equilibrium model can explain our experimental finding.

5. Summary

The target fragment yields, angular distributions and range distributions were measured using activation techniques for the reaction of 800 GeV protons with ^{197}Au. The results are consistent with previous measurements for the interaction of lower energy protons with ^{197}Au, in accord with limiting fragmentation.

The mass distribution agrees with the systematics of Sümmerer and Morrissey. The predictions of the microcanonical model for the statistical decay of highly excited nuclei are in general agreement with the measured mass distribution although the measured distribution did not have the oscillations in yields predicted by the model. The energy spectra of the spallation products were properly described using the DFF procedure and an initial fragment excitation energy spectrum from Glauber theory.

The authors gratefully acknowledge the E-772 Collaboration, Fermilab, for their help and assistance with the experiment. We also wish to thank Coreen Casey for helping with sample counting and Prof. G. Rudstam for helpful discussions. Financial support of the Swedish Natural Sciences Research Council, and the US Dept. of Energy through Grant No. DE-FG06-88ER40402 is gratefully acknowledged. One of us (H.R.J.) wishes to gratefully acknowledge the support from an Alexander von Humboldt fellowship.

References

1) W. Loveland, K. Aleklett, M. Bronikowski, Y.Y. Chu, J.B. Cumming, P.E. Haustein, S. Katcoff, N.T. Porile and L. Sihver, Phys. Rev. **C37** (1988) 1311
2) L.P. Remsberg and D.G. Perry, Phys. Rev. Lett. **35** (1975) 361
3) D.R. Fortney and N.T. Porile, Phys. Lett. **B76** (1978) 553
4) J.A. Urbon, S.B. Kaufman, D.J. Henderson and E.P. Steinberg, Phys. Rev. **C21** (1980) 1048
5) D.R. Fortney and N.T. Porile, Phys. Rev. **C21** (1980) 2511
6) S. Panadian and N.T. Porile, Phys. Rev. **C23** (1981) 427

7) J.S. Stewart and N.T. Porile, Phys. Rev. **C25** (1982) 478
8) N.T. Porile *et al.*, Phys. Rev. Lett. **43** (1979) 918
9) C.F. Wang and N.T. Porile, Phys. Rev. **C34** (1986) 1911
10) R.W. Stoennner, P.E. Haustein and J. Cumming, Phys. Rev. Lett. **53** (1984) 341
11) D.H.E. Gross, X.-Z. Zhang and S.-Y. Xu, Phys. Rev. Lett. **56** (1986) 1544
12) D.H.E. Gross and X.-Z. Zhang, Phys. Lett. **B161** (1985) 47
13) A.Y. Abul-Magd, D.H.E. Gross, S.-Y. Xu and Y.-M. Zheng, Z. Phys. **A325** (1986) 373
14) R.H. Kraus, Jr., *et al.*, Nucl. Phys. **A432** (1985) 525
15) K. Aleklett, W. Loveland, T. Lund, P.L. McGaughey, Y. Morita, G.T. Seaborg, E. Hagebø and I.R. Haldorsen, Phys. Rev. **C33** (1986) 885
16) D.J. Morrissey, W. Loveland, M. de Saint-Simon and G.T. Seaborg, Phys. Rev. **C21** (1980) 1783
17) D.J. Morrissey, D. Lee, R.J. Otto and G.T. Seaborg, Nucl. Instr. Meth. **158** (1978) 499
18) K. Aleklett, M. Johansson, L. Sihver, E. Loveland, H. Groening, P.L. McGaughey and G.T. Seaborg, Nucl. Phys. **A499** (1989) 591
19) S.I. Baker, C.R. Kerns, S.H. Pordes, J.B. Cumming, A. Soukas, V. Agoritsas and G.R. Stevenson, Nucl. Inst. Meth. **222** (1984) 467
20) K. Aleklett, to be published
21) K. Aleklett, Radiochemist's gamma ray table, 2nd ed., (OSU, 1987)
22) U. Reus and W. Westmeier, At. Data Nucl. Data Table **29** (1983) 1
23) S.B. Kaufman, E.P. Steinberg and M.W. Weisfield, Phys. Rev. **C18** (1978) 1349
24) S. Krämer, B. Neidhart and K. Bächmann, Inorg. Nucl. Chem. Lett. **13** (1977) 205
25) S.B. Kaufman and E.P. Steinberg, Phys. Rev. **C22** (1980) 167
26) K. Aleklett, L. Sihver and W. Loveland, Phys. Lett. **B197** (1987) 34
27) S.B. Kaufman, M.W. Weisfield, E.P. Steinberg, B.D. Wilkins and D. Henderson, Phys. Rev. **C14** (1976) 1121
28) G. Rudstam, Z. Naturforsch. **21a** (1966) 1077
29) K. Sümmerer and D.J. Morrissey, Proc. First. Int. Conf. on radioactive nuclear beams, ed. W.D. Myers, J.M. Nitschke and E.B. Norman, (World Scientific, Singapore, 1990) pp. 123–131
30) Particle Data Group, Rev. Mod. Phys. **56** (1984) S1;
S.P. Denisov, S.V. Donskov, Yu.P. Pokoshkin and D.A. Stoyanova, Nucl. Phys. **B61** (1973) 62
31) L.G. Northcliffe and R.S. Schilling, Nucl. Data Tables **7** (1970) 233
32) A.I. Warwick, H.H. Wieman, H.H. Gutbrod, M.R. Maier, J. Peter, H.G. Ritter, H. Stelzer and F. Weik, Phys. Rev. **C27** (1983) 1083
33) A.I. Warwick *et al.*, Phys. Rev. Lett. **48** (1982) 1719
34) V.P. Crespo and J. Cumming, Phys. Rev. **C2** (1970) 1777
35) P.L. McGaughey, W. Loveland, D.J. Morrissey, K. Aleklett and G.T. Seaborg, Phys. Rev. **C31** (1985) 896
36) D.J. Morrissey, Phys. Rev. **C39** (1989) 460
37) L. Winsberg, Phys. Rev. **C22** (1980) 2116; **22** (1980) 2123
38) W. Loveland, D.J. Morrissey, K. Aleklett, G.T. Seaborg, S.B. Kaufman, E.P. Steinberg, B.D. Wilkins, J.B. Cumming, P.E. Haustein and H.-C. Hseuh, Phys. Rev. **C23** (1981) 253
39) G.D. Cole and N.T. Porile, Phys. Rev. **C25** (1982) 244
40) J.B. Cumming, P.E. Haustein, and H.-C. Hseuh, Phys. Rev. **C24** (1981) 2161
41) C.J. Waddington and P.S. Friar, Phys. Rev. **C31** (1985) 888;
X. Campi, private communication
42) L. Wenzin, S. Tong, W. Dingquing, S. Rulin, Z. Lili, J. Genming, Z. Yuming, C. Tahai and S. Benhao, Proc. Int. Symp. on heavy ion physics, Lanzhou, October, 1990 (to be published)
43) D.H.E. Gross, Rep. Prog. Phys. (to be published)
44) D.H.E. Gross, G. Klotz-Engmann and H. Oeschler, Phys. Lett. **B224** (1989) 29
45) S.I. Baker, R.A. Allen, P. Yurista, V. Agoritsas and J.B. Cumming, Phys. Rev. **C43** (1991) 2862